Wang, Qiming; Pang, Cheng; Wang, Yuzhong; Sihvola, Ari; Qi, Jiaran

Non-Interleaved Wideband High Gain Tx/Rx Array Antenna with High Aperture Efficiency for In-Band Full-Duplex Systems

Published in:
IEEE Transactions on Antennas and Propagation

DOI:
10.1109/TAP.2024.3479732

E-pub ahead of print: 01/01/2024

Document Version
Peer-reviewed accepted author manuscript, also known as Final accepted manuscript or Post-print

Please cite the original version:
Wang, Q., Pang, C., Wang, Y., Sihvola, A., & Qi, J. (2024). Non-Interleaved Wideband High Gain Tx/Rx Array Antenna with High Aperture Efficiency for In-Band Full-Duplex Systems. *IEEE Transactions on Antennas and Propagation*. Advance online publication. https://doi.org/10.1109/TAP.2024.3479732

Non-Interleaved Wideband High Gain Tx/Rx Array Antenna With High Aperture Efficiency for In-Band Full-Duplex Systems

Qiming Wang, *Student Member*, *IEEE*, Cheng Pang, Yuzhong Wang, *Student Member*, *IEEE*, Ari Sihvola, *Life Fellow*, *IEEE*, and Jiaran Qi, *Senior Member*, *IEEE*

***Abstract*—A Tx/Rx non-interleaved array antenna for in-band full-duplex (IBFD) systems is proposed in this article. Distinct from the reported Tx/Rx interleaved arrays, the proposed array adopts a novel dual-mode radiation unit that can simultaneously operate in Tx and Rx manners, without requiring the decoupling elements between the Tx units and the Rx units, while arranging more radiation units to realize a higher aperture efficiency. The non-interleaved array consists of several full-duplex dual-mode units and a feed network. The dual-mode unit can simultaneously operate in the radiation-mode and reflection-mode at the same frequency. In radiation-mode, a high-gain array (Rx) can be constructed by combining the feeding network. In reflection-mode, a high-gain reflectarray (Tx) can be implemented by combining a spatial feed. The polarization statuses of the radiation-mode and reflection-mode are right-hand-circular-polarization (RHCP) and LHCP, respectively, which greatly decreases the self-interference between the Tx and Rx channels. The proposed IBFD array is designed, fabricated, and measured at *X*-band with an operating bandwidth of 23.1% and 35.2% in the Tx and Rx channels, respectively. The maximum gain in two channels is 23.1 dBic and 23.6 dBic with a high aperture efficiency of 50.8% and 58.1%. The passband isolation is higher than 35.0 dB.**

***Index Terms*—In-band full-duplex (IBFD), non-interleaved Tx/Rx array antenna, dual mode antenna unit, simultaneous transmit and receive (STAR), wideband high gain array antenna.**

I. Introduction

IN-BAND FULL-DUPLEX (IBFD) communication system has been extensively studied over the past few years since it can multiply the spectrum efficiency and greatly increase the throughput to cope with the congested spectrum resources [1]–[5]. In the IBFD systems, the communication terminals need to transmit and receive signals at the same frequency at the same time. Therefore, minimizing the self-interference (SI) between the Tx and Rx channels is necessary and challenging. Typically, the SI can be canceled in antenna-domain, analog-domain, and digital-domain [6]–[9].

At the antenna level, many approaches have been proposed to realize high isolation between the Tx and Rx channels. Using spatial isolation where the Tx and Rx antennas are separated by a large distance is the most direct way [10]–[12] while the area of the antenna system is too large. In addition, the decoupling approach is widely applied to design IBFD antennas [13]–[17]. By adding extra decoupling structures between the Tx and Rx antenna, high Tx/Rx isolation can be realized. The area of these IBFD antennas is typically larger than one wavelength which is not suitable for building an IBFD array. The widely considered approaches for designing high-gain IBFD array antennas can be classified into the following two types. One uses the same Tx/Rx radiation structure and the SI cancellation is completed by a Butler matrix beamforming network. Several 2 × 2 IBFD arrays are proposed based on this configuration [18]–[21]. In [18], an external feed network constructed by two 90° hybrids and four 180° hybrids is designed to cancel the coupled Tx voltage at the Rx port. Moreover, a 2 × 2 IBFD array based on a single-layer substrate is proposed which integrates the feed network and the radiation patch in the same layer [21]. These arrays realize high Tx/Rx isolation while a complex feeding network is necessary which may not be easy to implement a large-scale IBFD array. The other approach for building IBFD arrays is based on a four-arm spiral element whose periodicity is less than λ/2. In [22] and [23], this element is used to construct IBFD antennas with wide band high isolation. Highly symmetrical antenna structure is required to ensure a high Tx/Rx isolation. Two dummy ports and four Ferrite cores are additionally applied. Moreover, great caution must be paid in the soldering to guarantee the symmetry of antenna structures. Similar elements have also been applied in [24] and [25] to construct small-scale phased arrays. Despite the realized high performance, such an approach may not be suitable for implementing large-scale low-cost high-gain IBFD arrays which can be highly beneficial for satellite systems and signal repeaters.

Reflectarray is a good candidate for constructing large-scale high-gain antennas due to its easy deployment, low weight, and low cost advantages despite the increased profile resulting from the feed source. The reported IBFD reflectarray has three types of antenna configuration. The first one is the spatially separated Tx/Rx arrays [10] as depicted in Fig. 1(a) where two different arrays with a large spatial distance are adopted to realize a high gain beam in both Tx and Rx channels. In this architecture, the IBFD system occupies a larger space which may not be easy to realize integration in a space-constrained system. After that, a side-by-side Tx/Rx array antenna [26] is proposed to realize a

This paper was partially supported by National Natural Science Foundation of China under Grant no. 62271170, no. 61671178, and no. 62071152.

Q. Wang, C. Pang, Y. Wang, and J. Qi are with Microwave Engineering Dept., School of Electronics and Information Engineering, Harbin Institute of Technology, Harbin 150001, China (*Corresponding author: Jiaran Qi*, e-mail: qi.jiaran@hit.edu.cn). (Q. Wang and C. Pang contribute equally to this work.)

Ari Sihvola is with the Department of Electronics and Nanoengineering, Aalto University, 00076 Espoo, Finland.

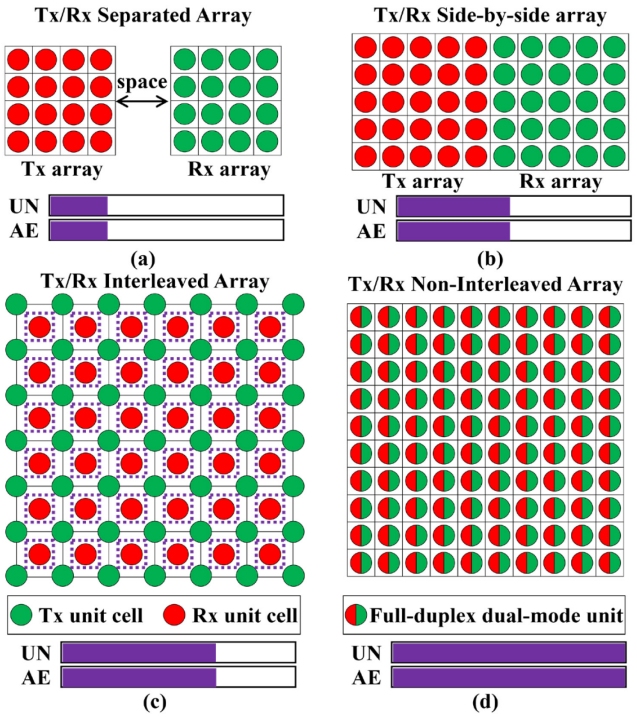

Fig. 1. (a) The Tx/Rx separated IBFD array configuration [10]. (b) The Tx/Rx side-by-side IBFD array [26]. (c) The Tx/Rx interleaved IBFD array antenna [28] (The purple dotted box represents the extra isolation elements between the Tx and Rx unit cells). (d) The proposed Tx/Rx non-interleaved array antenna with full-duplex dual-mode radiation unit cell. (UN represents the unit number under a given aperture size. AE represents the aperture efficiency of the array.)

more compact antenna system. The aperture layout is shown in Fig. 1(b). The Tx and Rx arrays are integrated into the same aperture without any spatial isolation. However, since only half of the aperture is operating for the Tx/Rx channel, the realized aperture efficiency is around half of the single antenna [27].

Recently, an aperture-shared IBFD reflectarray is proposed relying on a Tx/Rx interleaved radiation aperture [28]. The Rx units are interleaved between the Tx units as shown in Fig. 1(c). To reduce the mutual coupling between Tx units and Rx units, extra via fences are surrounded by the Rx unit. This architecture occupies the whole aperture in both Tx and Rx manners, more radiation unit cells can be arranged in the given aperture which further improves the realized aperture efficiency. Although the Tx/Rx interleaved array has realized impressive performance, it still faces the following inadequacies. Firstly, since the Tx and Rx units work at the same frequency, therefore, extra isolation structures are needed which increases the structure complexity and fabrication cost up to a point. Secondly, the interleaved Tx and Rx array result in an excessive unit periodicity for the Tx/Rx units which inevitably limits the realized gain and aperture efficiency of the array. Thirdly, two different types of Tx/Rx elements need to be co-designed and reasonably interleaved in a limited aperture which results in a higher design complexity. Finally, the –3 dB gain bandwidth is relatively narrow (10.0%) which results from the inherently narrow-band properties of the single patch mode and the resonance phase [29]. Although the Tx/Rx interleaved array realizes a quasi-monostatic IBFD array, the structural and antenna performance inadequacies resulting from interleaving are still significant. Therefore, a novel design approach to realize a Tx/Rx non-interleaved high-gain low-cost IBFD reflectarray with high aperture efficiency, low structural

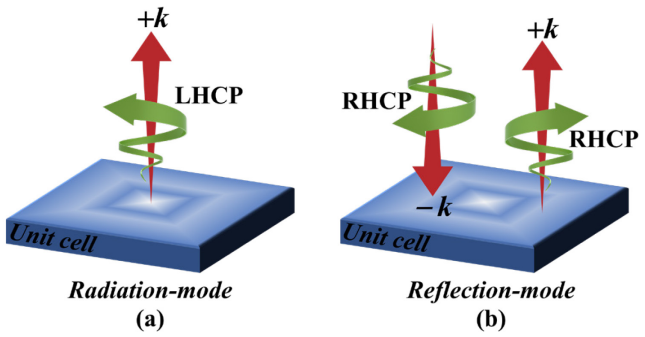

Fig. 2. (a) The radiation mode of the proposed full-duplex dual-mode unit (Rx). (b) The reflection mode of the proposed full-duplex dual-mode unit (Tx).

complexity, high reuse efficiency of the radiation elements, and wide gain bandwidth is worthy of being detailly investigated.

In this article, a novel Tx/Rx non-interleaved array antenna is proposed based on a full-duplex dual-mode radiation unit cell which can simultaneously operate in Tx and Rx manners at the same frequency. The arrangement of the units on the aperture is depicted in Fig. 1(d). It is found that the proposed architecture realizes IBFD capabilities at the unit cell level, each unit within the array can simultaneously transmit and receive (STAR) EM signals. The unit can thus have a suitable periodicity, more unit cells can hence be arranged in a specific aperture, and a higher antenna gain and aperture efficiency can be realized. The full-duplex radiation unit can simultaneously work in the radiation mode and reflection mode which is utilized to construct Rx and Tx channels, respectively. In radiation mode, the unit radiates LHCP waves. In reflection mode, the incidence RHCP waves will be fully reflected and reradiated to the space. The operating mechanism of the dual-mode element is depicted in Fig. 2. The operating polarization status of the reflection mode (RHCP) is orthogonal to the radiation mode (LHCP) which reduces the SI at the element level. By arranging this dual-mode element into an array, an IBFD array antenna with high aperture efficiency and high Tx/Rx isolation can be constructed.

II. Antenna Architecture and Operating Mechanism

A. Antenna architecture of the proposed IBFD array

The proposed Tx/Rx non-interleaved IBFD array antenna is illustrated in Fig. 3 which contains an array built by 16 × 16 full-duplex dual-mode unit cells, a 1–256 microstrip feeding network, and an RHCP horn antenna. In the Tx channel, the reflection mode of the unit cell is working and a reflectarray can be built by combining the RHCP feed. In the Rx channel, the radiation mode of the unit cell is working and an array antenna combined with the feeding network is constructed. The detailed view and zoom view of the radiation layer and the 1-to-256 feed work are depicted in Figs. 3(b)–(e), respectively.

B. Operation mechanism of the proposed IBFD array

When the Tx port is excited, the RHCP waves radiated from the horn antenna will illuminate the full-duplex array. Since the unit cells can only receive LHCP waves, the RHCP waves will be completely reflected and reradiated into the free space. No EM energy will flow from the feeding network to the Rx port, a high isolation between the Tx and Rx ports can thus be obtained. When the Rx port is excited, the EM energy will be distributed

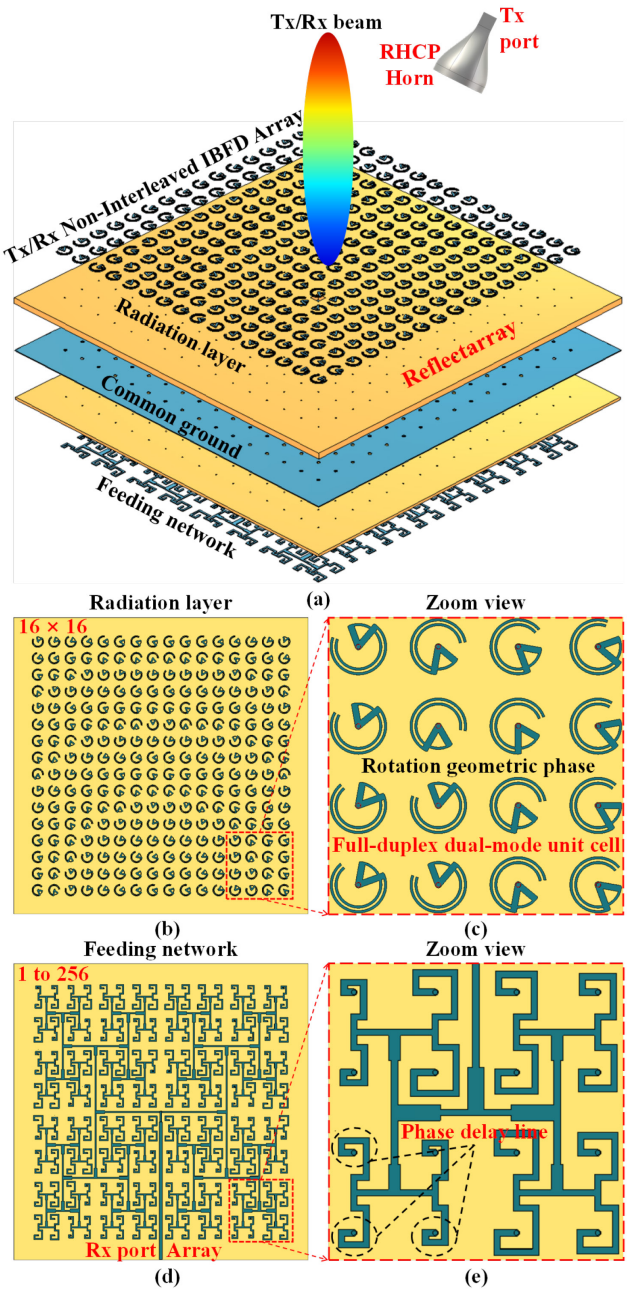

Fig. 3. (a) The exploded view of the proposed Tx/Rx non-interleaved wideband IBFD array antenna. (b) The top radiation layer of the IBFD array consists of 16 × 16 full-duplex dual-mode unit cells. (c) The zoom view of the top radiation layer. (d) The 1-to-256 microstrip feeding network of the IBFD array. (e) The zoom view of the feeding network.

to each unit cell and radiate LHCP waves. The horn antenna cannot receive any EM energy due to the polarization mismatch, high isolation between the Rx and Tx ports is hence realized. The proposed IBFD array achieves SI cancelation at the unit cell level relying on two different operation modes of the full-duplex unit cell.

To realize a high gain IBFD array, the reflectarray (Tx) needs to correct the phase distribution on the array which means each unit on the aperture needs to provide a specific reflection phase. In this paper, the reflection geometric phase [30] is adopted for the dual-mode unit cell to achieve 2π reflection phase coverage due to its broadband properties. The reflection phase variation can be achieved by rotating the radiation patch within the range of 0°–180°. As for the Rx array antenna, each unit is required to operate with the same radiation amplitude and radiation phase for a high-gain pencil beam. The rotation of the radiation patch not only changes the reflection phase in the reflection mode but also affects the radiation phase in the radiation mode. When the high gain reflectarray (Tx) is constructed, the array not only has a desired reflection phase distribution but also has an undesired initial radiation phase distribution. To realize a high gain array antenna, one should compensate for this undesired initial phase. To accomplish this, phase delay lines connected to the feeding network are applied to each unit cell which can introduce new freedom for modulating the radiation phase of the units. Since no EM energy flows into the feeding network in the reflection mode, the phase delay line does not change the reflection phase of the unit cell. By adjusting the length of the phase delay line connected to each unit, an identical radiation phase distribution can be achieved which is the desired phase distribution for the array (Rx). By combining the rotation of the radiation patch and the phase delay line, high gain can be achieved in both reflect-array (Tx) and array antenna (Rx). Detailed properties of the IBFD array antenna are introduced in the following sections.

III. Design of the Full-Duplex Dual-Mode Unit Cell

A. Topology of the full-duplex dual-mode unit cell

The design of the full-duplex dual-mode unit cell is the key part of implementing the non-interleaved IBFD array. The unit cell needs to simultaneously fulfill the functionalities shown in Fig. 2. As for the radiation mode (Fig. 2(a)), any type of LHCP element can be satisfied. As for the reflection mode (Fig. 2(b)), since the *cross-pol* excited waves (RHCP) cannot be received by the LHCP radiation element, therefore, no energies flow into the feeding structure which guarantees the low SI between the two modes. Next, to realize complete reflection, a metal ground is the easiest choice [31]. Therefore, the LHCP antenna element is preferred to have a metal ground. Further, to realize a planner array, the element is preferred to be the microstrip structure. In summary, a coaxial or microstrip-feeding planner LHCP patch antenna can be a better topology structure for constructing the full-duplex dual-mode unit cell. Since a feeding network is also needed, a microstrip-to-coaxial patch antenna shown in Fig. 4(a) is eventually adopted. This topology unit consists of three metal layers and two substrate layers. A via is adopted to connect the feeding line and the radiation patch. The patch is used to radiate LHCP waves in the radiation mode. The common ground offers complete reflection in the reflection mode.

In this article, to realize a broadband IBFD array antenna, a double circular open ring depicted in Fig. 4(b) is adopted as the radiation patch of the proposed dual-mode unit cell since it has two patch modes which can be combined into a wide bandwidth. The two open rings have different radii and both are connected to the central feed point by the microstrip stubs. The operating frequency of the circular rings can be modulated by its radius (r_1, r_2). The polarization of the unit cell can be modulated by the open angle of the circular rings (θ_1, θ_2). The middle layer and bottom layer of the unit cell are shown in Fig. 4(c) and Fig. 4(d), respectively. The input impedance of the microstrip feed line is set as 100 Ω for a thinner line width which reduces the mutual coupling in the feeding network. The ε_r of the substrate is 2.65 with a loss tangent of 0.001. The adopted dielectric material is

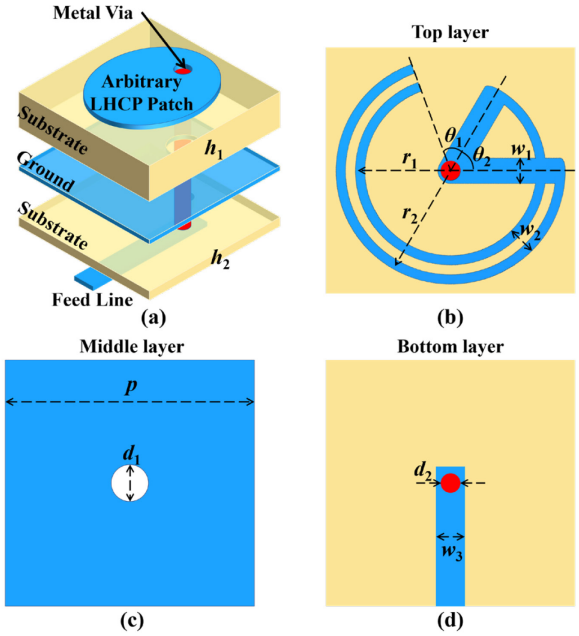

Fig. 4. (a) The topology structure of the full-duplex dual-mode unit cell. (b) The top layer of the proposed full-duplex dual-mode unit cell. (c) The middle layer of the unit cell. (d) The bottom layer (microstrip feeding line) of the unit cell. (r_1 = 2.8 mm, r_2 = 3.4 mm, w_1 = 0.8 mm, w_2 = 0.9 mm, θ_1 = 50°, θ_2 = 60°, h_1 = 2.8 mm, h_2 = 1.27 mm, P = 10 mm, d_1 = 0.6 mm, d_2 = 1.5, w_3 = 0.8 mm)

F4B. A Bondply with a ε_r of 4.2 and a thickness of 0.1 mm is used to connect two substrate layers.

B. Reflection mode and phase modulation

The proposed full-duplex dual-mode unit cell is simulated by the F-solver in the commercial software CST Microwave studio. The simulation model of the unit cell in the reflection mode is shown in Fig. 5(a). This simulation model contains three ports, Z_{max}, Z_{min}, and Waveguide Port 1. The Z_{max} and the Z_{min} ports can radiate RHCP and LHCP EM waves to excite the unit cell. The scattered EM waves from the unit cell can also be perfectly absorbed by these two ports. The Waveguide Port 1 is utilized to feed the unit cell, the guided EM waves generated by Port 1 can be transformed into radiated EM waves by the unit cell, and the radiated EM waves can be received by the Z_{max} and the Z_{min} ports. Period boundary conditions are applied to the unit cell.

To verify the polarization selectivity of the radiation patch, we simulated the electric field distribution of the unit cell when the Z_{max} port generates RHCP and LHCP waves, respectively. The simulated electric fields are illustrated in Fig. 6. For a clear observation, we hid the substrate and the common ground. As shown in Fig. 6(a), the generated LHCP waves excite a strong electric field on the radiation patch. The EM energy received by the patch flows into the feed line via the connected hole which demonstrates that the patch can radiate and receive LHCP EM waves. In Fig. 6(b), the generated RHCP EM waves also excite an electric field on the patch while no EM energy flows into the feed line due to the polarization mismatch. The incident waves reach the metal ground and will be fully reflected.

According to the electric field analysis, RHCP EM waves are adopted to excite the unit in the reflection mode. The simulated S-parameters between the Z_{max} port and the remaining ports are shown in Fig. 7. It is found that the unit cell provides a higher than 0.9 $S_{Zmax\,(R),\,Zmax\,(R)}$ within the frequency range of 9.4 GHz–

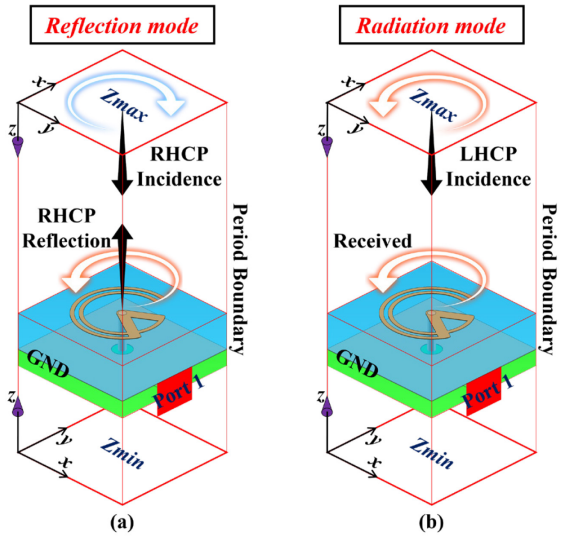

Fig. 5. (a) The simulation model of the proposed full-duplex dual-mode unit cell in the reflection mode (Tx) and (b) in the radiation mode (Rx).

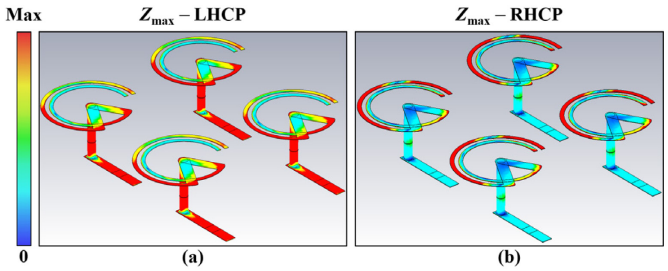

Fig. 6. (a) The simulated electric field distribution of the dual-mode unit cell in the radiation mode when the Z_{max} port generates LHCP EM waves and (b) generates RHCP EM waves. (The substrate layer and ground layer are hidden.)

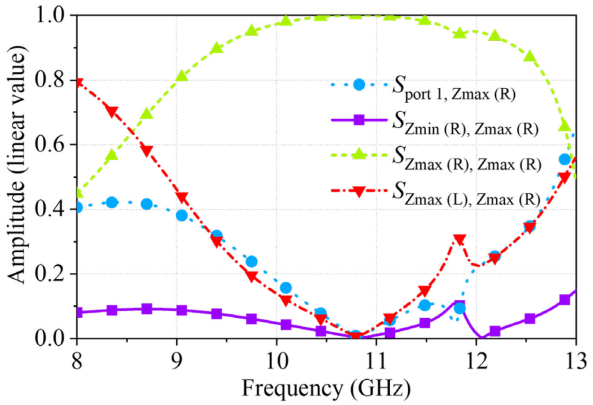

Fig. 7. The simulated S-parameters between the Z_{max} port, the Z_{min} port, and the waveguide Port 1 in the reflection mode.

12.4 GHz which verifies the reflection polarization conversion property of the unit cell. The *cross*-reflection amplitude ($S_{Zmax\,(L),\,Zmax\,(R)}$) and the transmission amplitude between the Z_{max} port and the remaining ports are all lower than 0.3 in this frequency range. The subscript Z_{max} represents the excitation port and the receive port. *R*/*L* indicates the RHCP and LHCP, respectively.

The reflection mode of the unit cell is utilized to construct the Tx reflectarray. To converge the RHCP waves radiated from the feed to a specific direction, each unit cell in the reflectarray is needed to offer a desired reflection phase. Therefore, the unit is supposed to provide a reflection phase range covering 2π. To modulate the reflection phase, the geometric phase method [30]

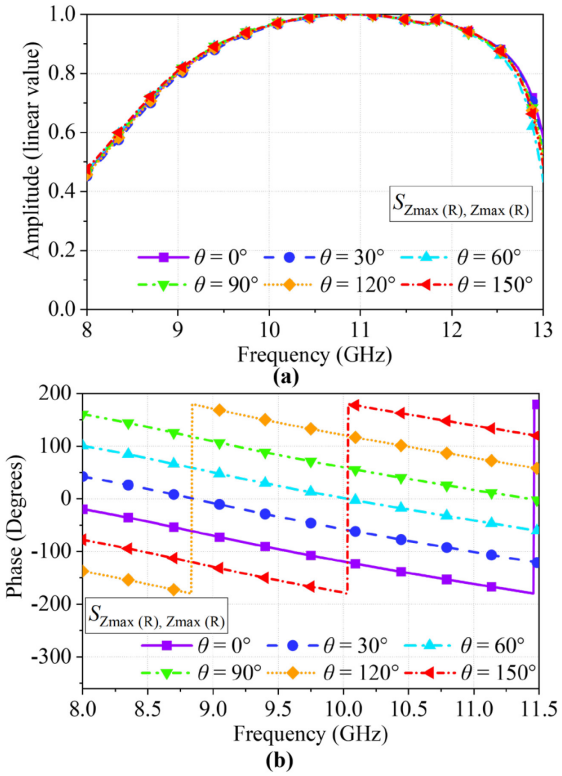

Fig. 8. (a) The simulated amplitude of the $S_{Zmax\ (R),\ Zmax\ (R)}$ under different angles. (b) The simulated phase of the $S_{Zmax\ (R),\ Zmax\ (R)}$ under different rotation angles.

is used in the reflection mode of the unit. By simply rotating the radiation patch with an angle of θ, a reflection phase fluctuation of 2θ is obtained. Therefore, the 2π reflection phase coverage can be achieved by rotating the patch within the θ range of 0°–180°. The simulated amplitude and phase of the $S_{Zmax\ (R),\ Zmax\ (R)}$ under different rotation angles are illustrated in Fig. 8. As can be found, the amplitude differs little and remains larger than 0.9 in a wide band. As the rotation angle varies, the almost linear phase curve is shifted. The reflection phase can cover 360° over the entire X-band. The wideband high reflection amplitude and full phase coverage ensure the wideband high gain performance of the Tx reflectarray.

C. *Radiation mode and phase modulation*

Next, the properties of the full-duplex dual-mode unit cell in the radiation mode are introduced. According to the electrical field analysis (Fig. 6(a)), the double circular patch can transmit and receive LHCP EM waves. The simulation model of the unit cell in the radiation mode is illustrated in Fig. 5(b). Due to the reciprocity of antenna transmit and receive, we have two ways to obtain the properties of the unit cell in the radiation mode. The first way is letting the unit cell operate in a transmit manner, i.e., the radiation patch is excited by the guided EM waves from Port 1 and radiates LHCP waves to free space, and the radiated waves are received by the Z_{max} port. The second way is letting the unit cell operate in a receive manner, i.e., the radiation patch is excited by the radiated LHCP energy from the Z_{max} port and guides EM energy into the feeding line, and the guide waves are received by Port 1. In this paper, we choose the second way to be consistent with the electric field analysis (Fig. 6).

Set the Z_{max} port to the excited state with LHCP EM energy emitted and the remaining ports to be matched, the properties of

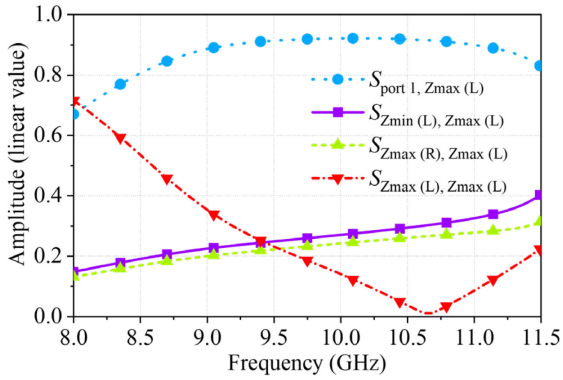

Fig. 9. The simulated S-parameters between the Z_{max} port, the Z_{min} port, and the waveguide Port 1 in the radiation mode.

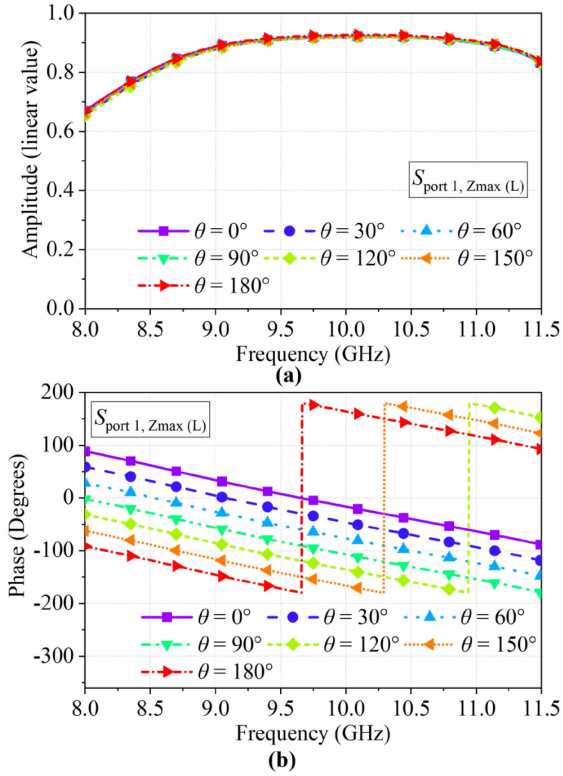

Fig. 10. (a) The simulated amplitude of the $S_{port\ 1,\ Zmax\ (L)}$ under different angles. (b) The simulated phase of the $S_{port\ 1,\ Zmax\ (L)}$ under different rotation angles.

the dual-mode unit in the radiation mode can be simulated. The simulated S-parameters in the radiation mode are shown in Fig. 9. As can be seen, the unit cell can efficiently receive the LHCP waves radiated from the Z_{max} port. The transmission coefficient between the Z_{max} port and port 1 ($S_{port\ 1,\ Zmax\ (L)}$) is higher than 0.8 within the range of 8.5 GHz–11.6 GHz. The wideband property of the unit cell in the radiation mode results from the adopted double circular radiation structure which has two patch modes. The *co-pol* reflection amplitude ($S_{Zmax\ (L),\ Zmax\ (L)}$) is lower than 0.3 within the frequency range of 9.2 GHz–11.6 GHz. At the lower band, the $S_{Zmax\ (L),\ Zmax\ (L)}$ increases which is mainly due to the imperfect impedance match between the excitation port and the unit cell. The *cross-pol* reflection amplitude ($S_{Zmax\ (R),\ Zmax\ (L)}$) is lower than 0.4 within the range of 8.2 GHz–11.6 GHz. Since the feed line on the bottom layer (Fig. 4(b)) will radiate a few EM waves to the free space, therefore, the $S_{Zmin\ (L),\ Zmax\ (L)}$ is not zero while this value is small within the operating bandwidth.

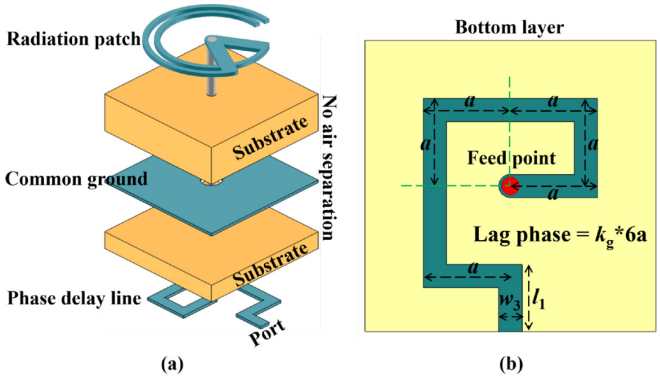

Fig. 11. (a) The 3-D view of the modified full-duplex dual-mode unit cell. (b) The structure of the bottom layer with an extra phase delay line.

The radiation mode of the unit cell is utilized to construct the Rx array antenna. For a high-gain array with a broadside pencil beam, each unit in the array is required to operate in the same state with an identical radiation phase. Since the Tx reflectarray requires the radiation patch of each unit with a specific rotation angle to offer a desired reflection phase distribution. Therefore, the units in the array cannot be in the same state which cannot directly offer the desired identical radiation phase distribution for constructing the array antenna. The rotation of the radiation patch can modulate the reflection phase while it can also adjust the radiation phase of the unit cell. For the 2π reflection phase coverage, the radiation patch is rotated within 0°– 180°. In this rotation range, the simulated $S_{\text{port 1, Zmax (}L\text{)}}$ is shown in Fig. 10. As can be found, the transmission amplitude differs little as the rotation angle varies. However, the radiation phase shifts as the rotation angle varies. When the radiation patch is rotated by θ, the radiation phase also fluctuates θ. Rotating the patch with the range of 0°–180° can obtain a radiation phase coverage of 0°–180° which is the radiation-type geometric phase [32].

As discussed above, both the reflection phase and radiation phase variations of the dual-mode unit are strongly correlated to the rotation angle of the patch. The desired parabolic reflection phase distribution for the Tx reflectarray and the same radiation phase distribution for the Rx array antenna cannot be satisfied at the same time using the current unit cell (Fig. 4(b)). A new phase modulation freedom is needed to decouple the geometric reflection phase and the geometric radiation phase.

D. Geometric phase decoupling in two operation modes

To break the correlations between the two types of geometric phases and the rotation angle of the radiation patch, the feeding line in the bottom layer of the unit (Fig. 4(d)) is modified which is added with an extra phase delay line. The modified unit cell is depicted in Fig. 11. Since the common ground separates the radiation patch and the feed structure, the newly added phase delay line will not affect the performance of the unit cell in the reflection mode. The geometric reflection phase of the unit cell is the same as discussed in Section III Part B. However, since the phase delay line is connected to the radiation patch, it will affect the radiation phase of the unit cell. By varying the length of the phase delay line, the radiation phase of the unit cell can be modulated. At this time, the reflection phase of the unit cell can only be modulated by rotating the radiation patch while the radiation phase of the unit can be modulated by both the phase delay line and the rotation angle of the patch. The phase delay

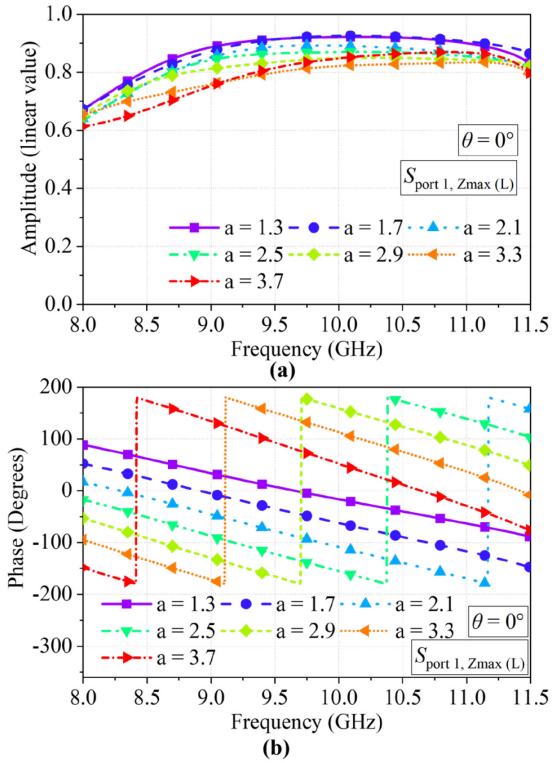

Fig. 12. (a) The simulated amplitude of the $S_{\text{port 1, Zmax (}L\text{)}}$ under different phase delay line lengths. (b) The simulated phase of the $S_{\text{port 1, Zmax (}L\text{)}}$ under different phase delay line lengths. (The unit of a is mm.)

line introduces new freedom for modulating the radiation phase of the unit cell while not affecting its reflection phase. With the phase delay line, the strong coupling of two geometric phases in two operation modes of the unit cell is successfully decoupled. The dual-mode unit cell can provide arbitrary radiation phases and arbitrary refection phases simultaneously by associatively regulating the rotation angle of the patch and the length of the phase delay line. By arranging this dual-mode unit into an array, the Tx reflectarray, and the Rx array antenna can hence realize their desired antenna performance.

The simulated $S_{\text{port 1, Zmax (}L\text{)}}$ of the unit with a specific rotation angle patch under different phase delay line lengths is shown in Fig. 12. As can be found, the transmission amplitude gradually decreases as the length of the phase delay line increases which is mainly due to the enhanced self-radiation of the phase delay line. Nevertheless, the transmission amplitude keeps larger than 0.8 within the frequency of 9.5 GHz–11.5 GHz in all modulated cases. As shown in Fig. 12(b), the transmission phase gradually lags as the length of the phase delay line increases. At a specific rotation angle of the radiation patch, the radiation phase covers 2π range by modulating the length of the phase delay line which completely breaks the dependence of the radiating phase on the rotation angle. The radiation phase of the unit cell equals the lag phase of the phase delay line plus the radiated geometric phase of the radiation patch. The lag phase can be applied to the units with arbitrary rotation angle patches.

IV. Implementation of the IBFD Array Antenna

A. S_{11} and radiation pattern of the element in Rx mode

Set Port 1 in the simulation model shown in Fig. 5(b) as the excitation state, the S_{11} and radiation patterns of the proposed

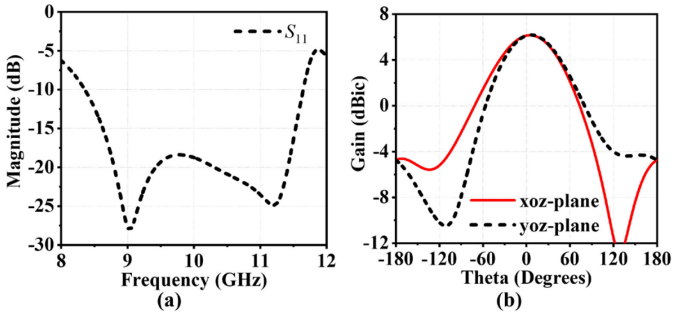

Fig. 13. The simulated S_{11} and radiation patterns of the element radiator in the radiation mode (Rx mode).

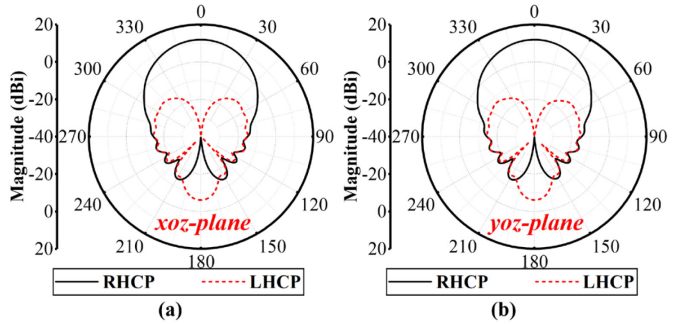

Fig. 14. (a) The simulated radiation patterns of the RHCP horn antenna in *xoz*-plane and (b) *yoz*-plane.

element in the radiation mode (Rx) can be obtained as depicted in Fig. 13. As can be seen, the S_{11} of the element remains lower than −10 dB within the range of 8.35–11.65 GHz. The relative bandwidth is 33.0%. Two resonance points occur which results from the double patch mode of the adopted radiation structure. The element realized a gain of 6.1 dBic at 11.0 GHz which is a normal gain for the microstrip patch antenna.

B. Spatial horn antenna for the reflectarray–Tx

An RHCP horn antenna is used to illuminate the reflectarray. Since the aperture efficiency of the reflectarray is highly related to the F/D (F is the focal length, D is the diameter), and the F/D is preferred to be around 0.5 [33], therefore, the horn antenna is needed to have a −10 dB beamwidth of around 90° to guarantee high excitation efficiency. An RHCP horn antenna [34] with a −10 dB beamwidth of 88.6° and a realized gain of 11.9 dBic at 10.6 GHz is designed. The simulated radiation patterns of the horn antenna are shown in Fig. 14. The simulated S_{11} and axial ratio of the RHCP horn are shown in Fig. 15. The horn antenna has a −10 dB S_{11} bandwidth of 8.7–14.3 GHz. The axial ratio is lower than 3.0 dB within the frequency range of 8.4–12.6 GHz. The proposed array consists of 16 × 16 unit cells. The aperture size is 160 mm × 160 mm. According to the beamwidth of the horn (88.6°), the F of the reflectarray can be ascertained as 82.0 mm. The F/D of the reflectarray is thus 0.51.

C. Reflection and radiation phase profile of the IBFD array

As for the construction of the high-gain IBFD array antenna, the parabolic reflection phase distribution can be first assigned to the Tx reflectarray to ascertain the rotation angle of each unit cell in the array. After that, the rotation angle of each unit will endow the array with an initial radiation phase distribution. To obtain an identical radiation phase distribution for achieving a high-gain Rx array, the phase delay line of each unit cell needs

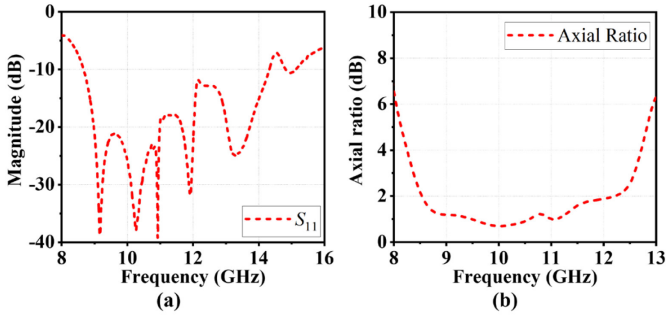

Fig. 15. The simulated S_{11} and axial ratio of the LHCP horn antenna.

to compensate for this initial radiation phase. Depending on the radiation phase to be compensated, the length distribution of the phase delay line can be determined eventually. At this point, both the reflection and radiation phase profiles required for the IBFD array can be fulfilled. The phase calculation procedure of the proposed array is shown in Fig. 16(a). The calculated results are introduced as follows.

As depicted in Fig. 16(b), to reduce the blocking effect, the RHCP horn antenna is placed 45 mm away along the *x*-axis and 82 mm away along the *z*-axis. To obtain a broadside high-gain pencil beam, the reflectarray is required to fulfill the following parabolic reflection phase distribution.

$$\varphi(x,y) = \mathrm{k}_0\left(\sqrt{(x-x_0)^2+(y-y_0)^2+z_0^{\,2}} - fd\right)$$
$$fd = \sqrt{x_0^{\,2}+y_0^{\,2}+z_0^{\,2}} \tag{1}$$

The horn antenna is placed at the focal point (x_0, y_0, z_0), and (x, y) is the position coordinate of each unit cell in the array. In (1), $x_0 = 45$, $y_0 = 0$, $z_0 = 82$. The calculated phase distribution is shown in Fig. 16(c). By matching the desired reflection phase with the reflection phase library shown in Fig. 8(b), the rotation angle of each unit cell can be ascertained. The rotation angle distribution on the array is shown in Fig. 16(d). The rotation angle is within the range of 0°–180°.

By rotating the radiation patch of each unit cell on the array, the desired reflection phase distribution for the Tx reflectarray is fulfilled. Since the rotation of the radiation patch also affects the radiation phase of the unit, according to the radiation phase results shown in Fig. 10(b), the rotation angle distribution (Fig. 16(d)) will give the array an initial radiation phase distribution which is illustrated in Fig. 16(e). To realize a broadside pencil beam for the Rx array antenna, each unit cell in the array needs an identical radiation phase. Set the desired radiation phase on the array as full 0°, the lag phase distribution to be compensated for by the phase delay line is the negative of the initial radiation phase. According to the lag phase results depicted in Fig. 12(b), the length distribution of the phase delay line on the array can be obtained which is illustrated in Fig. 16(f). By adding the lag phase and the initial radiation phase, the final radiation phase distribution on the array can be obtained which is illustrated in Fig. 16(g). It is seen that the radiation phase fluctuates around 0°. The maximum radiation phase difference on the array is 10° with an unevenness of around 5°. Although the final radiation phase profile is not perfectly identical, it is sufficient to build a high-gain array due to the negligible phase differences.

Finally, it is worth mentioning that the proposed dual-mode full-duplex unit can simultaneously offer any desired reflection phase and radiation phase, more attractive performances of the

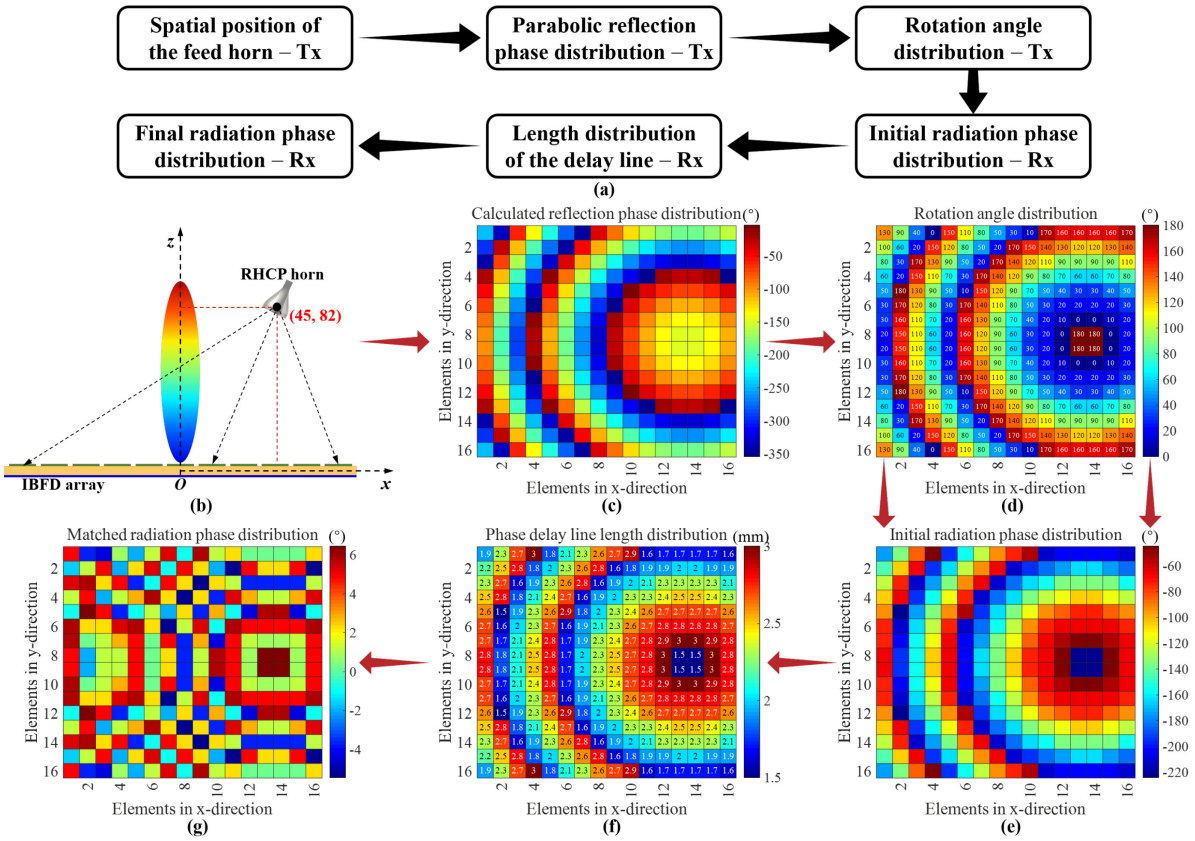

Fig. 16. (a) The phase calculation procedure of the proposed IBFD array. (b) The spatial position of the Tx reflectarray and the RHCP horn. (c) The calculated reflection phase distribution of the array at 10.6 GHz. (d) The patch rotation angle distribution on the reflectarray at 10.6 GHz. (e) The initial radiation phase distribution of the array at 10.6 GHz. (f) The length distribution of the delay line on the array. (g) The matched radiation phase distribution on the array at 10.6 GHz.

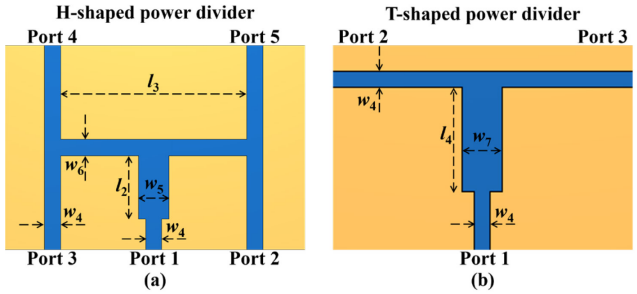

Fig. 17. (a) The structure of the H-shaped power divider. (b) The structure of the T-shaped power divider. (w_4 = 0.8 mm, w_5 = 1.5 mm, w_6 = 0.8 mm, w_7 = 2 mm, l_2 = 3.1 mm, l_3 = 9.2 mm, l_4 = 5.25 mm)

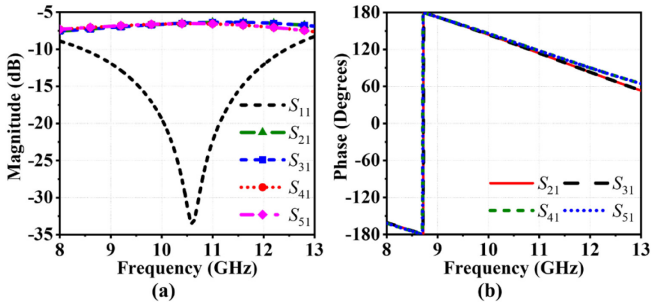

Fig. 18. (a) The simulated transmission amplitude performance of the H-shaped power divider. (b) The phase performance of the H-shaped power divider.

IBFD array antenna can be realized by endowing the array with different phase profiles, such as IBFD beam steering array for signal repeaters/boosters, and IBFD orbital angular momentum (OAM) generator for a larger channel throughput.

D. Feeding network for the radiation array–Rx

A microstrip 1-to-256 feeding network is designed to excite the 16 × 16 radiation array. The whole feeding network shown in Fig. 3(d) is implemented with 64 H-shaped 1-to-4 power dividers and 62 T-shaped 1-to-2 power dividers. The H-shaped power divider and the T-shaped power divider are illustrated in Fig. 17(a) and Fig. 17(b), respectively. Both the H-shaped and T-shaped power dividers are supposed to realize identical phase output. The four output ports of the H-shaped power divider are connected to the phase delay line of the radiation unit cell in the array. The simulated transmission performance of the H-shaped power divider is shown in Fig. 18. As can be seen, the S_{11} of the input port is less than −10 dB within the frequency range of 8.5 −12.5 GHz. The amplitude imbalance and phase imbalance of the four output ports are less than 0.64 dB and 9.1°, respectively within the range of 8.5–12.5 GHz. The simulated transmission properties of the T-shaped power divider are shown in Fig. 19. The S_{11} of the input port is less than −10 dB within the range of 8.0–14.0 GHz. The amplitude and phase of the two output ports are identical. The input impedance of all ports of the H-shaped and T-shaped power divider is 100 Ω for a thinner line width. A 50 Ω microstrip feeding line is adopted for the final Rx port for more convenient measurement.

It is worth mentioning that the H-shaped and T-shaped power dividers are only used to provide an equal feeding phase for all

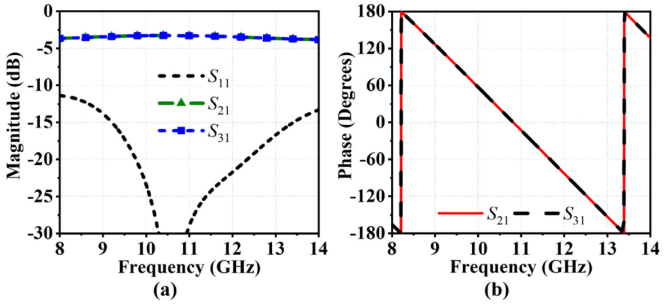

Fig. 19. (a) The simulated transmission amplitude performance of the T-shaped power divider. (b) The phase performance of the T-shaped power divider.

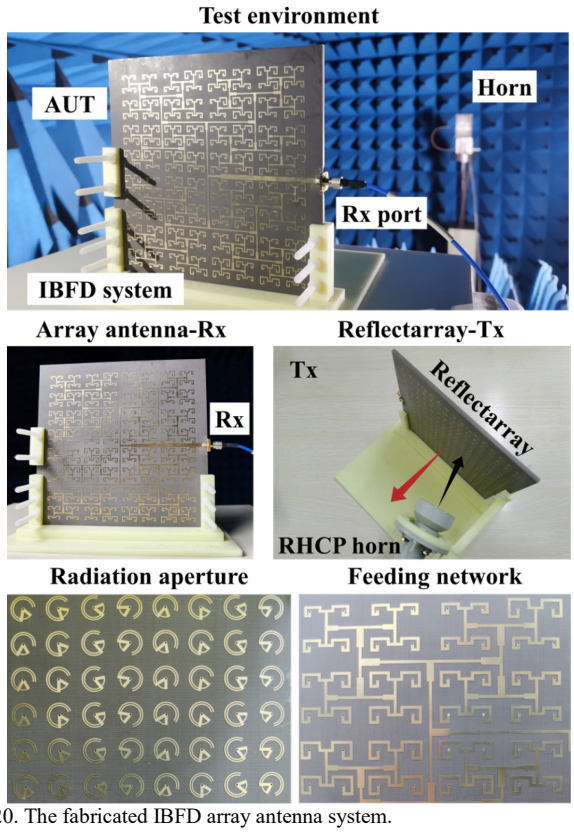

Fig. 20. The fabricated IBFD array antenna system.

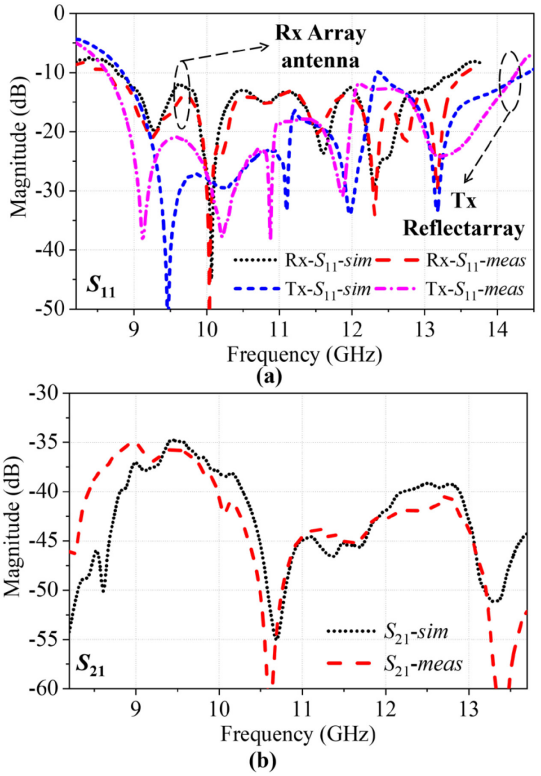

Fig. 21. (a) The simulated and measured S_{11} of the proposed IBFD array. (b) The simulated and measured S_{21} of the proposed IBFD array antenna.

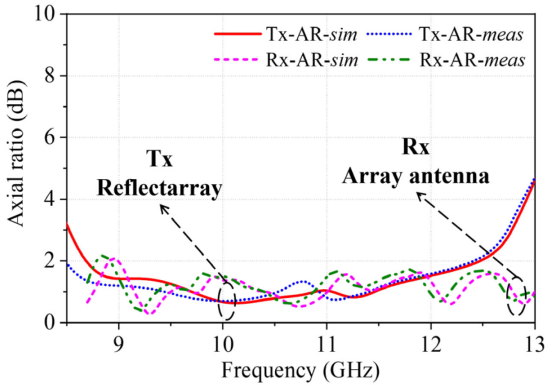

Fig. 22. The simulated and measured axial ratio of the IBFD array.

the radiation elements in the array. High output port isolation is dispensable in the designed feeding network. We analyzed the output port isolation of the designed power divider. Since there is no isolation structure, the output port isolation is poor while this will not affect the Tx/Rx isolation of the overall antenna.

V. Experimental Performance and Comparison

A. Fabricated antenna prototype and measurement results

To validate the proposed Tx/Rx non-interleaved IBFD array configuration, a proof-of-concept prototype antenna fabricated by the printed-circuit-board technology and an antenna holder fabricated by the 3D-printed technology are assembled to be an IBFD antenna system. The fabricated antenna system is shown in Fig. 20. The input impedance of the Tx and Rx ports are all 50 Ω. The antenna is tested in the microwave anechoic chamber. Fig. 21 shows the simulated and measured S_{11} and S_{21} of the Tx reflectarray and the Rx array antenna. As can be seen, the S_{11} of the reflectarray is less than −10 dB within the frequency range of 8.9–14.4 GHz. The −10 dB S_{11} bandwidth of the Rx array is ranging from 8.8 GHz to 13.4 GHz. The isolation between the Tx and Rx ports is better than 35.0 dB within the range of 8.2–13.7 GHz. A maximum isolation of 55.3 dB is achieved at 10.7 GHz. The simulated S-parameters of the array agree well with the measured results. The slight frequency shift results from the fabrication and assemble tolerance.

The simulated and measured axial ratio of the IBFD array is shown in Fig. 22. It can be seen that the Tx reflectarray has a 3-dB axial ratio bandwidth of 40.4% (8.5 GHz–12.8 GHz). As for the Rx array antenna, thanks to the adopted broadband radiation patch, the axial ratio is less than 2.1 dB within the bandwidth of 44.6% (8.7 GHz–13.7 GHz). The wideband low axial ratio thus ensures the wideband high isolation level between the Tx and Rx ports which is highly desired in the IBFD systems.

The simulated and measured realized gain of the IBFD array is shown in Fig. 23. The Tx reflectarray realizes a wideband –3

TABLE I
COMPARISON AMONG THE PROPOSED IBFD ARRAY ANTENNA AND OTHER IBFD ARRAY ANTENNAS

Reference	Antenna Configuration	Polarization Frequency	3-dB Gain Bandwidth	Maximum Gain (dB)	Passband Isolation	Array Size (Scale)	Aperture Efficiency	Antenna Profile	Complexity & Cost
[18]	Radiation array–Butler matrix BFN network	Circularly 2.5 GHz	Tx: 4.1% Rx: 4.1%	9.0 dBic 10.0 dBic	> 47.0 dB > 47.0 dB	1.7λ × 1.7λ 4-element	22.8% 28.6%	Low	High–Butler BFN network
[21]	Radiation array–Butler matrix BFN network	Circularly 2.5 GHz	Tx: 4.1% Rx: 4.1%	10.5 dBic 10.5 dBic	> 41.0 dB > 41.0 dB	1.9λ × 1.9λ 4-element	22.8% 28.6%	Low	High–Butler BFN network
[22]	Radiation array–High symmetry spiral element	Circularly 2.0 GHz	Tx: 50.0% Rx: 50.0%	12.5 dBic 12.5 dBic	> 27.0 dB > 27.0 dB	2.8λ × 2.5λ 7-element	27.0% 27.0%	Low	High–Ferrite Dummy ports
[23]	Radiation array–High symmetry spiral element	Circularly 3.3 GHz	Tx: NA Rx: NA	15.0 dBic 15.0 dBic	> 35.0 dB > 35.0 dB	2.5λ × 2.5λ 25-element	39.8% 39.8%	Low	High–Ferrite Dummy ports
[10]	Reflectarray–Tx/Rx array spatially separated	Linearly 5.8 GHz	Tx: NA Rx: NA	15.0 dBi 17.1 dBi	> 38.7 dB > 49.5 dB	11.6λ × 2λ 384-element	11.5% 18.6%	High	Low–Tx/Rx Separated
[26]	Reflectarray–Tx/Rx array side-by-side	Linearly 15.0 GHz	Tx: 13.3% Rx: 13.3%	25.1 dBi 25.1 dBi	> 35.0 dB > 35.0 dB	15λ × 12λ 476-element	17.7% 17.7%	High	Low–Tx/Rx Side-by-side
[27]	Reflectarray–Tx/Rx array side-by-side	Linearly 94.5 GHz	Tx: 2.3%* Rx: 2.3%*	31.86 dBi 30.88 dBi	> 55.0 dB > 55.0 dB	11.3λ × 11.3λ 2670-element	31.4% 25.1%	High	Low–Tx/Rx Side-by-side
[28]	Reflectarray–Tx/Rx array interleaved	Circularly 28.0 GHz	Tx: < 5.0% Rx: < 9.0%	19.6 dBic 27.1 dBic	> 39.7 dB > 39.7 dB	9.7λ × 9.7λ 256-element	7.7% 43.4%	High	High–Tx/Rx Interleaved
Proposed	**Reflectarray**–Tx/Rx array **non-interleaved**	Circularly 10.6 GHz	Tx: **23.1**% Rx: **35.2**%	23.1 dBic 23.6 dBic	> 35.0 dB > 35.0 dB	5.7λ × 5.7λ **256**-element	**50.8**% **58.1**%	High	**Low–Non-interleaved**

(1) NA is not available. (2) 2.3%* in reference [27] represents the 1-dB gain bandwidth, the 3-dB gain bandwidth is not available.

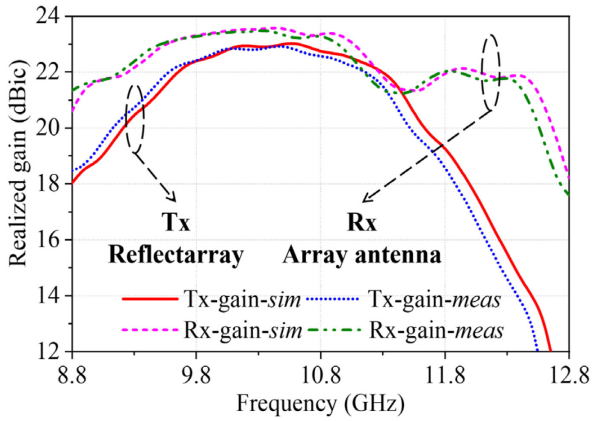

Fig. 23. The simulated and measured realized gain of the IBFD array.

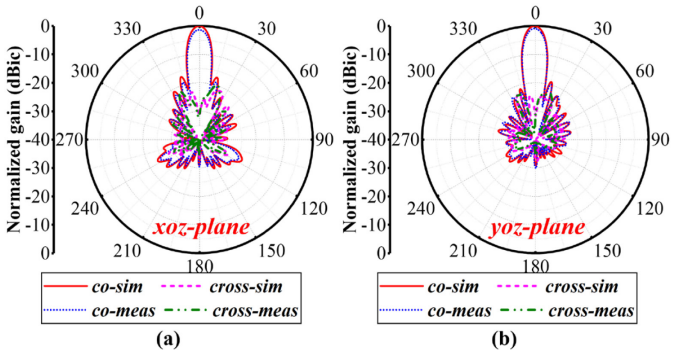

Fig. 24. (a) The simulated and measured radiation patterns of the reflectarray in the xoz-plane and (b) in the yoz-plane.

dB gain bandwidth of 23.1% (9.2 GHz–11.6 GHz) which is due to the broadband properties of the geometric phase. Compared with the resonance phase utilized in [28] to satisfy the reflection phase distribution, the geometric phase can easily realize wide-band phase modulation by rotating the radiation patch. The Rx array realizes a wideband –3 dB gain bandwidth of 35.2% (8.9 GHz–12.7 GHz) which results from the double patch mode of the radiation unit cell. The wideband radiation structure and the geometric reflection phase together empower the IBFD antenna broadband operating bandwidth in both Tx and Rx channels. In addition, as shown in Fig. 22, the proposed IBFD array realizes a maximum gain of 23.1 dBic at 10.6 GHz in the Tx manner. A closer maximum gain of 23.6 dBic has also been realized by the Rx array at 10.5 GHz. The aperture size of the proposed array in the simulation is 160 mm × 160 mm. The aperture efficiency of the antenna is calculated by the following formulation.

$$AE = \frac{G\lambda^2}{4\pi S} \tag{2}$$

AE is the calculated aperture efficiency, G is the antenna gain, λ is the wavelength, and S is the area. The corresponding aperture efficiency of the proposed array in the Tx and Rx manner are 50.8% and 58.1%, respectively. The similar gain performance in two manners and high aperture efficiency of the proposed IBFD antenna results from the Tx/Rx non-interleaved antenna architecture. The number and periodicity of the Tx and Rx radiation units are identical in the proposed IBFD array which makes it easier to adapt to more practical application scenarios. As analyzed above, the matched bandwidth (–10 dB S_{11}, 3-dB axial ratio, –3 dB realized gain) of the proposed IBFD array are 23.1% and 35.2% in the Tx and Rx channels, respectively.

The simulated and measured radiation patterns of the IBFD array in the Tx and Rx channels are depicted in Fig. 24 and Fig. 25, respectively. The side lobe level of the Tx reflectarray in the xoz-plane and yoz-plane are –17.0 dB and –18.9 dB. The cross-

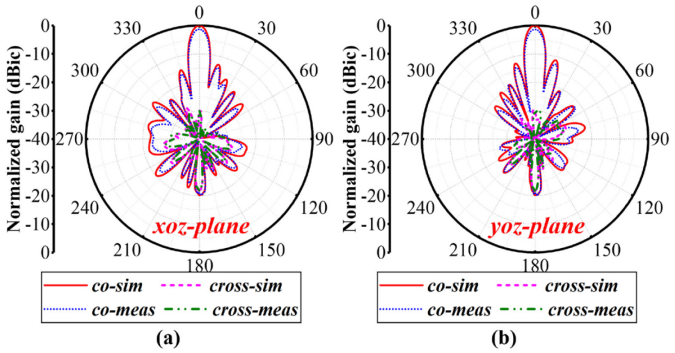

Fig. 25. (a) The simulated and measured radiation patterns of the Rx array in the xoz-plane and (b) in the yoz-plane.

polarization level of the reflectarray is better than −22.4 dB in both planes. As for the Rx array antenna, the side lobe level and cross-polarization level are lower than −12.9 dB and −21.6 dB in both planes, respectively. The side lobe level of the radiation array is relatively high which mainly results from the imperfect identical radiation phase distribution (Fig. 16(g)). In addition, the backward radiation of the radiation array is −20.0 dB which is acceptable, however, compared with the Tx reflectarray, this value is relatively high which mainly results from the radiation of the feeding network. The simulated radiation efficiency and total efficiency of the Tx reflectarray are 98.8% and 95.2% at 10.6 GHz, respectively. As for the radiation array, the radiation efficiency and total efficiency are 99.4% and 94.3%.

B. Comparison among the reported IBFD arrays

The comparison between the previously reported IBFD array and the proposed antenna is shown in Table I. Compared with the IBFD radiation array shown in the orange part of the Table, the proposed array antenna features a higher aperture efficiency, a larger array scale, lower structure complexity, and lower cost. Due to the complicated Butler matrix feeding network [18], [21] and high demand on the symmetry of the antenna structure [23], [25], these IBFD radiation arrays are inconvenient for building large-scale array antennas despite their lower antenna profile. Compared with the IBFD reflectarray shown in the blue part of the Table, thanks to the adopted Tx/Rx non-interleaved antenna architecture, more Tx/Rx elements can be arranged on a given aperture, and the highest aperture efficiency is realized in both channels. In addition, since both the Tx and Rx channels utilize the same dual-mode radiation element, no additional isolation structures [28] are required, the antenna complexity and system cost are relatively low. Moreover, the proposed array realized the widest −3 dB gain bandwidth due to the adopted broadband radiation element and the geometric phase. As for the passband isolation, the proposed IBFD array realized a larger than 35.0 dB isolation in the whole band which is an acceptable value. By increasing the F/D which means the distance between the feed of the reflectarray and the radiation array is larger, the isolation can be further increased.

VI. Conclusion

A Tx/Rx non-interleaved IBFD array based on a full-duplex dual-mode radiation unit cell is proposed. The dual-mode unit cell can simultaneously transmit and receive EM signals at the same frequency. The SI cancelation between the Tx and the Rx channels is realized by means of the different polarization states of the two operation modes at the unit cell level. By arranging the dual-mode unit into an array and combining it with a horn and a feed network, a Tx reflectarray, and an Rx array antenna are constructed sharing each radiation unit cell in the array. An IBFD array antenna operating at the *X*-band with a bandwidth of 23.1% in the Tx channel and a bandwidth of 35.2% in the Rx channel is designed, fabricated, and measured. The IBFD array achieved an aperture efficiency of 50.8% in the Tx channel and 58.1% in the Rx channel. The isolation between the Rx and Tx channels is higher than 35 dB in the whole working bandwidth. The high aperture efficiency, wide bandwidth, low complexity, and low system cost properties of the proposed IBFD array can potentially boost the commercialization of the IBFD systems. It is worth mentioning that since the proposed IBFD array works in two orthogonal polarizations, it can also be applied in dual-polarization scenarios with high polarization isolation while the traditional dual-polarized antenna may not be readily utilized in the IBFD systems due to insufficient isolation.

References

[1] C. B. Barneto et al., "Full-duplex OFDM radar with LTE and 5G NR waveforms: Challenges solutions and measurements," *IEEE Trans. Microw. Theory Techn.*, vol. 67, no. 10, pp. 4042–4054, Oct. 2019.

[2] K. E. Kolodziej, B. T. Perry, and J. S. Herd, "In-band full-duplex technology: Techniques and systems survey," *IEEE Trans. Microw. Theory Techn.*, vol. 67, no. 7, pp. 3025–3041, Jul. 2019.

[3] A. Sabharwal, P. Schniter, D. Guo, D. W. Bliss, S. Rangarajan, and R. Wichman, "In-band full-duplex wireless: Challenges and opportunities," *IEEE J. Sel. Areas Commun.*, vol. 32, no. 9, pp. 1637–1652, Sep. 2014.

[4] Y.-M. Zhang and J.-L. Li, "Differential-series-fed dual-polarized traveling-wave array for full-duplex applications," *IEEE Trans. Antennas Propag.*, vol. 68, no. 5, pp. 4097–4102, May 2020.

[5] C. Ye, Y.-M. Zhang, J.-L. Li, G. F. Pedersen, and S. Zhang, "High-isolation dual-polarized leaky-wave antenna with fixed beam for full-duplex millimeter-wave applications," *IEEE Trans. Antennas Propag.*, vol. 69, no. 11, pp. 7202–7212, Nov. 2021.

[6] T. Dinc and H. Krishnaswamy, "A T/R antenna pair with polarization-based reconfigurable wideband self-interference cancellation for simultaneous transmit and receive," in *IEEE MTT-S Int. Microw. Symp. Dig.*, May 2015, pp. 1–4.

[7] J. Zhong, E. A. Alwan, and J. L. Volakis, "Ultra-wideband dual-linear polarized phased array with 60◦ scanning for simultaneous transmit and receive systems," in *Proc. Int. Workshop Antenna Technol., Small Antennas, Innov. Struct., Appl. (iWAT)*, 2017, pp. 140–141.

[8] J. P. Doane, K. E. Kolodziej, and B. T. Perry, "Simultaneous transmit and receive with digital phased arrays," in *Proc. IEEE Int. Symp. Phased Array Syst. Technol. (PAST)*, Oct. 2016, pp. 1–6.

[9] S. Khaledian, F. Farzami, B. Smida, and D. Erricolo, "Inherent self-interference cancellation for in-band full-duplex single-antenna systems," *IEEE Trans. Microw. Theory Techn.*, vol. 66, no. 6, pp. 2842–2850, Jun. 2018.

[10] A. Samaiyar, A. H. Abdelrahman, and D. S. Filipovic, "Simultaneous transmit and receive reflectarray antennas on low cost UAV platforms," in *Proc. IEEE Int. Symp. Antennas Propag. USNC/URSI Nat. Radio Sci. Meeting*, Jul. 2017, pp. 2047–2048.

[11] E. Everett and A. Sabharwal, "Spatial self-interference isolation for in-band full-duplex wireless: A degrees-of-freedom analysis," 2015, *arXiv:1506.03394*.

[12] E. Everett, A. Sahai, and A. Sabharwal, "Passive self-interference suppression for full-duplex infrastructure nodes," *IEEE Trans. Wireless Commun.*, vol. 13, no. 2, pp. 680–694, Jan. 2014.

[13] L. Sun, Y. Li, Z. Zhang, and Z. Feng, "Compact co-horizontally polarized full-duplex antenna with omnidirectional patterns," *IEEE Antennas Wireless Propag. Lett.*, vol. 18, no. 6, pp. 1154–1158, Jun. 2019.

[14] K.-Z. Hu, M.-C. Tang, Y. Wang, D. Li, and M. Li, "Compact, vertically integrated duplex filtenna with common feeding and radiating SIW cavities," *IEEE Trans. Antennas Propag.*, vol. 69, no. 1, pp. 502–507, Jan. 2021.

[15] R.-S. Chen et al., "High-isolation in-band full-duplex cavity-backed slot antennas in a single resonant cavity," *IEEE Trans. Antennas Propag.*, vol. 69, no. 11, pp. 7092–7102, Nov. 2021.

[16] J.-Y. Lin, Y. Yang, S.-W. Wong, and R.-S. Chen, "In-band full-duplex filtering antenna arrays using high-order mode cavity resonators," *IEEE Trans. Microw. Theory Techn.*, vol. 71, no. 4, pp. 1630–1639, Apr. 2023.

[17] Q. Tan and K. -M. Luk, "Wideband Co-Linearly Polarized Magneto-Electric Dipole Antenna for In-Band Full-Duplex Applications," *IEEE Trans. Antennas Propag.*, vol. 71, no. 2, pp. 1907–1912, Feb. 2023.

[18] J. Ha, M. A. Elmansouri, P. Valale Prasannakumar, and D. S. Filipovic, "Monostatic Co-Polarized Full-Duplex Antenna With Left- or Right-Hand Circular Polarization," *IEEE Trans. Antennas Propag.*, vol. 65, no. 10, pp. 5103–5111, Oct. 2017.

[19] M. A. Elmansouri, L. B. Boskovic, and D. S. Filipovic, "Compact Wideband Dual-Polarized In-Band Full-Duplex Antenna Subsystem," *IEEE Trans. Antennas Propag.*, vol. 69, no. 11, pp. 7166–7172, Nov. 2021.

[20] E. A. Etellisi, M. A. Elmansouri, and D. S. Filipovic, "Wideband Monostatic Co-Polarized Co-Channel Simultaneous Transmit and Receive Broadside Circular Array Antenna," *IEEE Trans. Antennas Propag.*, vol. 67, no. 2, pp. 843–852, Feb. 2019.

[21] Z. Zhou, Y. Li, J. Hu, Y. He, Z. Zhang, and P. -Y. Chen, "Monostatic Copolarized Simultaneous Transmit and Receive (STAR) Antenna by Integrated Single-Layer Design," *IEEE Antennas Wireless Propag. Lett.*, vol. 18, no. 3, pp. 472–476, Mar. 2019.

[22] M. A. Elmansouri, A. J. Kee, and D. S. Filipovic, "Wideband antenna array for simultaneous transmit and receive (STAR) applications," *IEEE Antennas Wireless Propag. Lett.*, vol. 16, pp. 1277–1280, 2017.

[23] A. Hovsepian, E. A. Alwan, and J. L. Volakis, "A Wideband, Scanning Array of Four-Arm Spiral Elements for Simultaneous Transmit and Receive," *IEEE Antennas Wireless Propag. Lett.*, vol. 19, no. 4, pp. 537–541, Apr. 2020.

[24] E. A. Etellisi, M. A. Elmansouri, and D. S. Filipovic, "Wideband monostatic simultaneous transmit and receive (STAR) antenna," *IEEE Trans. Antennas Propag.*, vol. 64, no. 1, pp. 6–15, Jan. 2016.

[25] E. A. Etellisi, M. A. Elmansouri, and D. S. Filipovi´c, "Wideband simultaneous transmit and receive (STAR) circular array system," in *Proc. Int. Symp. IEEE Phased Array Syst. Technol.*, Waltham, MA, USA, 2016, pp. 1–5.

[26] Q.-C. Ye, J.-L. Li, and C. Wang, "Development of microstrip reflectarray based monostatic STAR antenna," *AEU Int. J. Electron. Commun.*, vol. 137, Jul. 2021, Art. no. 153827.

[27] R. S. Hao, Y. J. Cheng, Y. F. Wu, and Y. Fan, "A W-band low-profile dual-polarized reflectarray with integrated feed for in-band full-duplex application," *IEEE Trans. Antennas Propag.*, vol. 69, no. 11, pp. 7222–7230, Nov. 2021.

[28] A. Samaiyar, M. Elmansouri, and D. S. Filipovic, "Shared-Aperture Reflectarrays and Antenna Arrays for In-Band Full-Duplex Systems," *IEEE Trans. Antennas Propag.*, vol. 71, no. 11, pp. 9095–9100, Nov. 2023.

[29] Hou-Tong Chen, Antoinette J Taylor, and Nanfang Yu, "A review of metasurfaces: physics and applications," *Reports on Progress in Physics*, vol. 79, no. 7, Jun. 2016.

[30] Y. Li *et al*., "Wideband Dual-Circularly-Polarized Reflect-Arrays Based on Dual-Functional-Layer Cells With Berry-Phase Compensation at X-Band," *IEEE Trans. Antennas Propag.*, vol. 70, no. 10, pp. 9924–9929, Oct. 2022.

[31] A. Ericsson *et al*., "A Contoured-Beam Reflector Satellite Antenna Using Two Doubly Curved Circular Polarization Selective Surfaces," *IEEE Trans. Antennas Propag.*, vol. 69, no. 2, pp. 658–671, Feb. 2021.

[32] W. Yang, K. Chen, J. Zhao, T. Jiang, and Y. Feng, "A Wideband High-Efficiency Transmit-Reflect-Array Antenna for Bidirectional Radiations With Distinct Circular Polarizations Based on a Metasurface," *IEEE Trans. Antennas Propag.*, vol. 71, no. 4, pp. 3695–3700, Apr. 2023.

[33] T. -J. Li, G. -M. Wang, T. Cai, H. -P. Li, J. -G. Liang, and J. Lou, "Broadband Folded Transmitarray Antenna With Ultralow-Profile Based on Metasurfaces," *IEEE Trans. Antennas Propag.*, vol. 69, no. 10, pp. 7017–7022, Oct. 2021.

[34] A. Mahmoud, A. A. Kishk, Z. Hao, and W. Hong, "Ka-band circularly polarized reflectarray: Using a double-layers cross slot," *IEEE Antennas and Propagation Magazine*, vol. 58, no. 4, pp. 60–68, Aug. 2016.

Qiming Wang was born in May 1999, Gansu, China. He received B.S. in Microwave Technology in Harbin Institute of Technology (HIT), China, in 2021. He is currently pursuing the Ph.D. degree at HIT. He has published three IEEE TAP papers and three IEEE AWPL papers. His research interests include Fabry-Perot Cavity antenna, multi-band high gain antennas, and In-Band Full-Duplex communication systems.

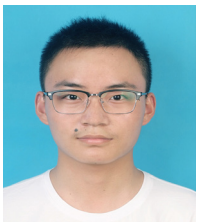

Cheng Pang was born in December 1999, Jiangsu, China. He received B.S. in Microwave Technology in Harbin Institute of Technology (HIT), China, in 2021. He is currently pursuing the Ph.D. degree at HIT. His research interests include multifunctional antennas, complex-amplitude metasurfaces, and metasurface inverse design.

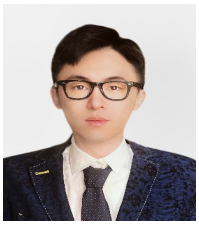

Yuzhong Wang was born in September 1999, Harbin, China. He received the B.S. degree in Microwave Technology at Harbin Institute of Technology (HIT), China, in 2021. He is currently pursuing the Ph.D. degree at HIT. His current research interests mainly include multifunctional metalens, inverse design metasurface, and deep diffraction neural networks.

Ari Sihvola (Life Fellow, IEEE) received the degrees of Diploma Engineer in 1981, Li-centiate of Technology in 1984, and Doctor of Technology in 1987, all in electrical engineering, from the Helsinki University of Technology (TKK), Espoo, Finland.

He is a Professor of electromagnetics with the School of Electrical Engineering (former name before 2010: Helsinki University of Technology), Aalto University, Espoo, Finland, with interest in electromagnetic theory, complex media, materials modeling, remote sensing, and radar applications. He is author and coauthor of several books, journal articles, and conference publications in electro-magnetics, homogenization principles, and metamaterials. He has given several plenary, keynote, and tutorial talks in international conferences. He served as Academy Professor (the distinguished professor status granted by the Academy of Finland) during the years 2005–2010. He was the Director of the national Graduate School of Electronics, Telecommuni-cations, and Automation, throughout 2008–2013. Starting from 2006, he is Chairman of the Finnish National Committee of URSI (International Union of Radio Science). He served as Chairman for the Commission B of International URSI during 2014–2017, and presently as Vice President and Treasurer of URSI. Distinguished Lecturer of IEEE Antennas and Propagation Society in 2013–2015. He is a fellow of URSI and the Electromagnetics Academy.

Jiaran Qi (Senior Member, IEEE) received the B.S. degree in communication engineering and the M.S. degree in electromagnetic field and microwave technology from Harbin Institute of Technology, Harbin, China, in 2004 and 2006, respectively. He the Ph.D. degree in electromagnetics from Aalto University, Finland, in 2011.

In January 2013, he joined Harbin Institute of Technology and is currently a professor and director of Department of Microwave Engineering. From October 2011 to September 2012, he conducted postdoctoral research in Department of Radio Science and Engineering, Alto University. He has co-authored more than 70 peer-reviewed journal and conference papers. His research interests include metasurface-based imaging, metamaterial-based antennas, and electromagnetic and circuit modeling of complex structures.